Microstructural and phase configurational effects determining water content:
Dielectric relationships of aggregated porous media

J. M. Blonquist Jr.,[1] S. B. Jones,[1] I. Lebron,[1,2] and D. A. Robinson[1,2]

[1]   Many porous media in which we determine water content are aggregated and characterized by a dual-porosity pore network, composed of interaggregate pores and intra-aggregate pores. This paper reports sample-scale permittivity measurements made in four stable aggregate media with dual porosity. Results indicate two distinct dielectric responses depending on whether the aggregates are surrounded by water or air. We relate transitions in the permittivity response to the water retention characteristic (WRC), showing that after the interaggregate pores have drained, the slope of the water content–permittivity relationship is significantly reduced (permittivity values ranging from 5 to 7). The hydraulic critical water content (θ_{hc}) is defined as the point where all the interaggregate pores are air filled and all the intra-aggregate pores are water saturated and is determined from the WRC. The dielectric critical water content (θ_{dc}) is defined as the point where a slope change in the measured water content–permittivity relationship occurs. A two-step model is presented and designed to capture the physical characteristics of the permittivity response to drainage. Measurements of θ_{hc} and θ_{dc} reveal a separation in these two values. The difference is considered to be a function of the connectivity of the intra-aggregate pore network. A connectivity ratio is defined as $1-(\theta_{dc}/\theta_{hc})$, where values close to 0 indicate low connectivity between the intra-aggregate pores and values tending to 1 indicate a high level of connectivity. Results from this work indicate that the reduced permittivity response measured in the water content–permittivity relationship is due to microstructure and phase configuration and not to "bound" water.

1. Introduction

[2]   Water content is a required parameter for estimating many processes in the vadose zone, and can be used to estimate changes in soil water storage in the water balance for many agronomic, ecological and hydrological applications. In an effort to link hydrology with soil structural information, electromagnetic (EM) geophysical instrumentation is increasingly used to characterize the subsurface. Methods ranging from active microwave remote sensing [*Dubois et al.*, 1995; *Ulaby et al.*, 1996; *Blumberg et al.*, 2000; *Du et al.*, 2000], to ground penetrating radar [*Chanzy et al.*, 1996; *van Overmeeren et al.*, 1997; *Binley et al.*, 2001; *Huisman et al.*, 2001; *Alumbaugh et al.*, 2002] and electromagnetic induction [*Lesch et al.*, 2005] are commonly used for this purpose. Much of the success of EM techniques dates to the seminal work of *Hoekstra and Delaney* [1974] and *Topp et al.* [1980], who recorded a firm relationship between water content (θ) and the effective

(bulk) permittivity (ε_b) of soils. During the past 25 years much attention and research effort has been focused on the development of EM techniques for estimating θ in porous media. One of the reasons for such wide application of EM sensors is their ease of use and broad applicability to a range of hydrological scales of interest. Instruments have been developed for sample-scale measurement such as time domain reflectometry (TDR) [*Noborio*, 2001; *Jones et al.*, 2002; *Robinson et al.*, 2003b], time domain transmission (TDT) [*Blonquist et al.*, 2005], impedance probes [*Hilhorst et al.*, 1993; *Gaskin and Miller*, 1996; *Seyfried and Murdock*, 2004] and capacitance probes [*Dean et al.*, 1987; *Paltineanu and Starr*, 1997; *Kelleners et al.*, 2004].

[3]   The work by *Topp et al.* [1980] for soils and the TDR measurement method has been widely adopted. However, deviation from the *Topp et al.* [1980] empirical calibration (equation (7)) has been demonstrated for clay soils [*Dobson et al.*, 1985; *Dirksen and Dasberg*, 1993; *Bridge et al.*, 1996]. This behavior is generally ascribed to the presence of bound water [*Dobson et al.*, 1985; *Dirksen and Dasberg*, 1993; *Wraith and Or*, 1999], or water held near solid surfaces due to interfacial interaction forces. Bound water undergoes dielectric saturation reducing its permittivity (ε) to the high-frequency value, $\varepsilon_\infty \approx 4.8$. Empirical [*Roth et al.*, 1992; *Jacobsen and Schjønning*, 1993; *Malicki et al.*, 1996; *Yu et al.*, 1997] and semiphysical [*Dirksen and*

---

[1]Department of Plants, Soils and Biometeorology, Utah State University, Logan, Utah, USA.
[2]Now at Department of Geophysics, Stanford University, Stanford, California, USA.

Dasberg, 1993; *Friedman*, 1998; *Or and Wraith*, 1999] models have tried to incorporate this, often by estimating bound water content based on the surface area of the material. Some of these models [*Wraith and Or*, 1999; *Or and Wraith*, 1999] have also explored temperature and frequency effects on bound water content and subsequent permittivity reductions in the water content–bulk permittivity ($\theta - \varepsilon_b$) relationship.

[4] Bound water has essentially become a convenient fitting parameter in models where the $\theta - \varepsilon_b$ calibration deviates below the *Topp et al.* [1980] calibration. However, the dielectric response of a mixture of dielectric components is complex and depends not only on the permittivity of the water phase, but also on bulk density/porosity [*Friedman*, 1998], structural configuration [*Jones and Friedman*, 2000; *Friedman and Jones*, 2001; *Robinson and Friedman*, 2001; *Cosenza et al.*, 2003; *Cosenza and Tabbagh*, 2004] and electrochemical properties [*Ishida and Makino*, 1999; *Logsdon*, 2005], some of which vary with frequency. The importance of water phase configuration in porous media was demonstrated using measurements in wet clays, polymers, potato powder, grains, corn starch and an aggregated Andisol soil [*Palmer*, 1952; *Stuchly*, 1970; *Jones and Or*, 2002; *Miyamoto et al.*, 2003]. Previous measurements demonstrated that complex grain structure and volcanic soils with high amounts of allophane minerals have internal porosity and exhibit permittivity values well below the *Topp et al.* [1980] calibration describing mineral soils. For many of the multipore structured media, a unique permittivity response is exhibited where the slope of the $\theta - \varepsilon_b$ relationship decreases at a water content that corresponds relatively well to the point where interaggregate pores are dry and the intra-aggregate pores are water saturated. The typical suggested reason for this response is the presence of adsorbed water in the intra-aggregate pores [*Palmer*, 1952; *Stuchly*, 1970; *Miyamoto et al.*, 2003]. In subsequent work, *Miyamoto et al.* [2005] presented an extension of the *Friedman* [1998] composite spheres model to 4 spherical layers [*Miyamoto et al.*, 2005, equations (4)–(13)]. By adjusting the weighting functions in the model they could achieve a reasonable fit with their measured data in Andisols.

[5] In this work we present a comprehensive data set for rigid, stable, dual-porosity aggregates with water retention characteristics (WRCs) and permittivity measurements of the variably saturated materials. Unraveling the dielectric response due to interacting phenomena aids the development of more sophisticated models to describe the $\theta - \varepsilon_b$ relationship. The aim of this work was to establish the contribution of dielectric phase configuration to the bulk permittivity response of aggregated materials in order to improve θ determination. The objective was to demonstrate the effects of microstructure and phase configuration on the $\theta - \varepsilon_b$ relationship in aggregated porous media, and to link the permittivity response of draining aggregates to the WRC through a permittivity model derived from first principles.

2. Theoretical Considerations

[6] Aggregate systems often form a dual-porosity pore network, which can be divided into interaggregate pores surrounding the aggregates, and intra-aggregate pores within the aggregates. The WRC of such materials differs considerably from a system containing a discrete granular matrix [*Durner*, 1994]. This dual-porosity system can be modeled using a bimodal function consisting of superpositioned van Genuchten water retention functions [*Durner*, 1994; *Kosugi et al.*, 2002]:

$$S_e = \sum_{i=1}^{k} w_i \left[\frac{1}{1 + (\alpha_i |h|)^{n_i}} \right]^{1 - \frac{1}{n_i}} \quad (1)$$

where $S_e = (\theta - \theta_r)/(\theta_s - \theta_r)$, θ_r is the residual volumetric water content, θ_s is the saturated volumetric water content, h is the matric head [m], α_i [m^{-1}] and n_i are curve fitting parameters relating to the matric head at air entry and pore size distribution, respectively [*van Genuchten*, 1980], w_i are weighting factors for each pore system and $k = 2$ for a bimodal WRC. When modeling the interaggregate pore system, θ varies from θ_s ($h = 0.0$ m) to the hydraulic critical water content (θ_{hc}), which is defined as the point where all the interaggregate pores are air filled and all the intra-aggregate pores are water saturated. When modeling the intra-aggregate pore system, θ varies from θ_{hc} to θ_r ($h < -100000$ m). The weighting factor $w_i = 1$ when modeling both the interaggregate and intra-aggregate pore systems.

[7] On the basis of the WRC, pore size distributions (f) are calculated according to

$$f(h) = \frac{d\theta(h)}{d \log_{10} |h|}. \quad (2)$$

The pore size distributions calculated with equation (2) can be plotted versus pore radius (r) [m], which is related to h according to

$$r = \frac{2\sigma \cos \gamma}{\rho_w g |h|} \quad (3)$$

where σ [N m^{-1}] and ρ_w [kg m^{-3}] are the temperature dependent surface tension and density of water, respectively, and are taken from *Weast* [1986], g is the acceleration of gravity [9.80 m s^{-2}] and γ is the contact angle (=0 for water).

[8] The presence of a dual-porosity pore system presents an interesting dielectric problem in terms of the phase configuration. The mixture consists of solid (ε_S), water (ε_W) and air (ε_A), with bound water (ε_{bw}) often being considered a fourth phase. In this analysis bound water is ignored and the three primary phases are dealt with. Conceptually, we outline five important physical conditions, or stages, of the porous medium (Figure 1): (1) The medium is completely dry. (2) The intra-aggregate pores are partially saturated but the interaggregate pores are air filled. (3) At θ_{hc} intra-aggregate pores are water saturated and all interaggregate pores are air filled. (4) The intra-aggregate pores are water saturated and the interaggregate pores fill with water under gravity, creating a layered system that has water-saturated interaggregate pores at the base and air-filled interaggregate pores at the top. (5) Both intra and interaggregate pores are water saturated and there is no air in the material.

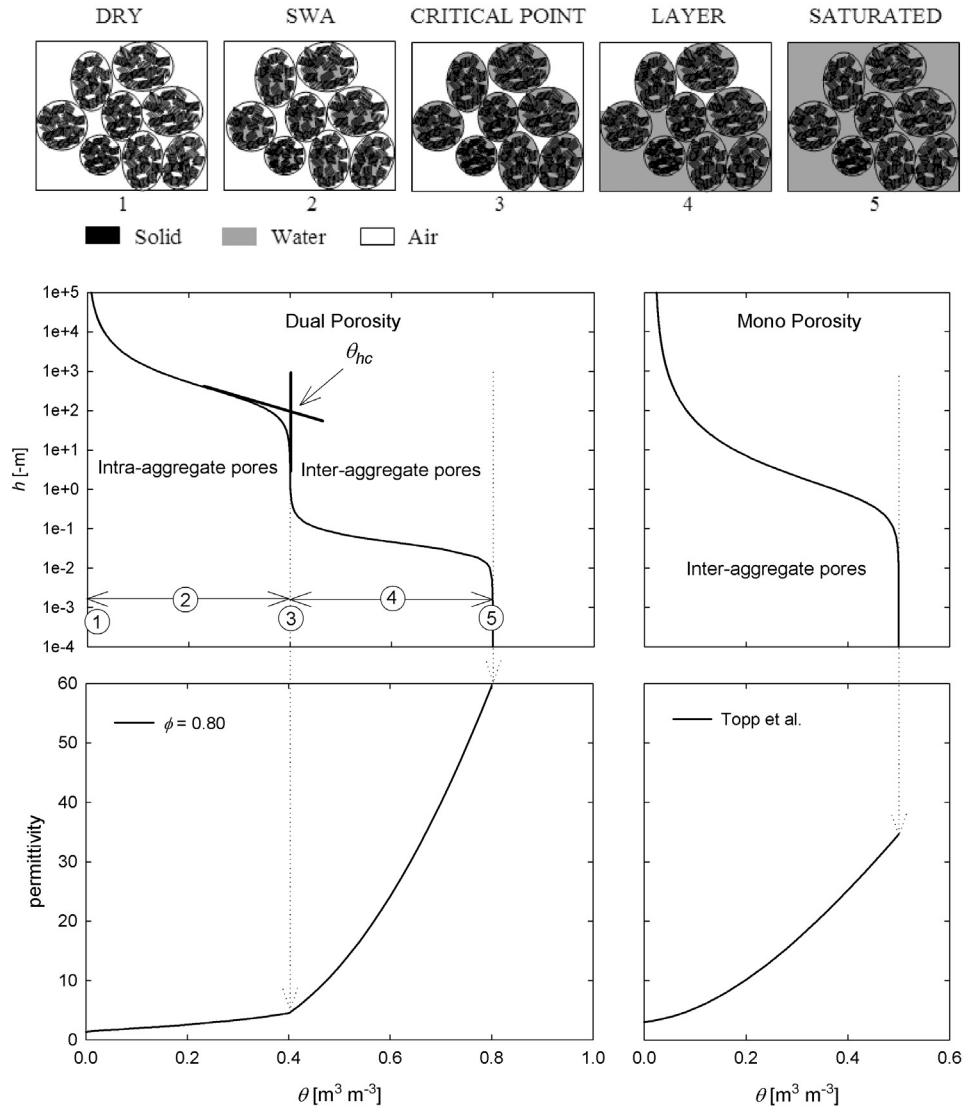[9] A saturated system (stage 5) can be considered to consist of water and solid; the water saturates both the

Figure 1. Schematic describing aggregate structure and illustrating the five described physical conditions (stages). The boundary between intra-aggregate and interaggregate pores on the water release characteristic (WRC) for a dual-porosity system corresponds to the hydraulic critical water content (θ_{hc}), stage 3. Stages 1 and 5 are the dry and saturated boundaries, respectively, and stages 2 and 4 represent the two draining, or wetting, portions of the WRC. At θ_{hc} (stage 3) a change in the permittivity response is expected because all the water in the sample is held in intra-aggregated pores. Equations (4)−(6) are used to model the permittivity response assuming $\varepsilon_W = 80$, $\varepsilon_S = 5$, $\varepsilon_A = 1$, $\theta_{hc} = \phi_i = \phi_e = 0.4$, $\theta = 0.8-0.4$ (equation (5)), $\varepsilon_{agg} = 48$, $\varepsilon_{sat} = 60$, $\varepsilon_{unsat} = 4.5$, $f_W = 0.4-0.0$ (equation (6)), and $f_S = 0.2$. A WRC and the permittivity response [*Topp et al.*, 1980] (equation (7)) for a mono porous system are shown for comparison.

interaggregate pores and the intra-aggregate pores ($\theta = \theta_s$). Treating a single aggregate as a two phase composite material, we estimate the permittivity of the water-saturated aggregate from the well known *Maxwell-Garnett* [1904] mixing formula:

$$\varepsilon_{agg} = \varepsilon_W + 3f_i\varepsilon_W\left(\frac{\varepsilon_S - \varepsilon_W}{\varepsilon_S + 2\varepsilon_W - f_i(\varepsilon_S - \varepsilon_W)}\right) \qquad (4)$$

where f_i is the volumetric fraction of the solid inclusions ($=1 - \phi_i$, where ϕ_i is the intra-aggregate porosity), ε_{agg} is the effective permittivity of the two-phase aggregate mixture, ε_W is the permittivity of the background water phase and ε_S is the permittivity of the solid. The model assumes that the solid inclusions are spherical and have noninteracting fields, thus we expect our model to be an upper bound for the permittivity. Equation (4) can be applied a second time, replacing ε_{agg} with ε_{sat}, giving an estimate of the bulk permittivity of a water-saturated sample of aggregates; where ε_S in equation (4) is replaced by ε_{agg} calculated from equation (4) under the first application and ϕ_i is replaced with the interaggregate porosity (ϕ_e). Applying equation (4) for a material with a total porosity of 0.8 and ϕ_i and $\phi_e = 0.4$, we can calculate $\varepsilon_{agg} = 48$ (single aggregate) and $\varepsilon_{sat} = 60$

(water-saturated aggregate composite material). Interestingly, this intuitive, physically based, two-step mixing approach, results in the same answer as a single step, and may be reduced to the simple problem of solid surrounded by water.

[10] The next step is to consider what happens as the composite material drains (stage 4). As the interaggregate pores are large, they drain easily and the material can be divided into two discrete layers; an upper layer that has saturated aggregates surrounded by air and a lower layer that has saturated aggregates surrounded by water. The ε_b of the system can be modeled as two dielectric layers, similar to the method described by *Robinson et al.* [2005] for coarse granular materials:

$$\sqrt{\varepsilon_b} = \sqrt{\varepsilon_{sat}}\left(\frac{\theta - \theta_{hc}}{\phi_e}\right) + \sqrt{\varepsilon_{unsat}}\left(1 - \left(\frac{\theta - \theta_{hc}}{\phi_e}\right)\right) \quad (5)$$

where θ is the mean volumetric water content, θ_{hc} is the water content at the hydraulic critical point determined from the WRC and ϕ_e is the interaggregate porosity. The permittivity of the saturated aggregate layer (ε_{sat}) is determined using equation (4). The permittivity of the unsaturated aggregate layer (ε_{unsat}) is anchored from the soil-water-air (SWA) calculation in the next modeling step.

[11] Once all the interaggregate pores have drained, the phase configuration of the system alters as the intra-aggregate pores begin to drain (stages 3-1). At this point the interaggregate pores are all filled with air and surround the aggregates which are a composite of solid, water and air. We tested a number of mixing approaches, including a two-step approach, but found that the most intuitive approach, using a dielectric shell model, consisting of solid surrounded by water surrounded by air [*Friedman*, 1998; *Sihvola*, 1999], captured the trend of the data the best. This simplified configuration allows continuity between the air and water phase and the solid and water phase as the aggregates dry, and is realistic as these phases always remain in contact. This configuration, SWA, was proposed by *Friedman* [1998] in his dielectric composite spheres model for soils and can be calculated according to

$$\varepsilon_{SWA} = \varepsilon_A$$
$$+ \left(\begin{array}{l} \{3\varepsilon_A[(f_S + f_W)(\varepsilon_W - \varepsilon_A)(2\varepsilon_W + \varepsilon_S) - f_S(\varepsilon_W - \varepsilon_S)(2\varepsilon_W + \varepsilon_A)]\}\cdot \\[6pt] \left[(2\varepsilon_A + \varepsilon_W)(2\varepsilon_W + \varepsilon_S) - 2\left(\dfrac{f_S}{f_S + f_W}\right)(\varepsilon_W - \varepsilon_A)(\varepsilon_W - \varepsilon_S) - (f_S + f_W)\cdot \right.^{-1} \\[6pt] \left.(\varepsilon_W - \varepsilon_A)(2\varepsilon_W + \varepsilon_S) + f_S(\varepsilon_W - \varepsilon_S)(2\varepsilon_W + \varepsilon_A)\right] \end{array}\right) \quad (6)$$

where the outer shell of each sphere has permittivity ε_A (air phase), the middle shell has permittivity ε_W (water phase), the inner shell has permittivity ε_S (solid phase) and f_S and f_W are the volume fractions of the solid and water phases, respectively. As the water phase vanishes, this model reduces to the two-phase Maxwell-Garnett model (equation (4)) with air surrounding solid. Parameters were assumed and calculated for equations (4)–(6) as follows: $\varepsilon_W = 80$, $\varepsilon_S = 5$, $\varepsilon_A = 1$, $\theta_{hc} = \phi_i = \phi_e = 0.4$, $\theta = 0.8-0.4$ (equations (5)), $\varepsilon_{agg} = 48$, $\varepsilon_{sat} = 60$, $\varepsilon_{unsat} = 4.5$, $f_W = 0.4-0.0$ (equation (6)) and $f_S = 0.2$, and the permittivity response of a hypothetical dual-porosity medium was simulated with the proposed model (Figure 1).

[12] In the graphs of Figure 1 we compare the WRCs of a dual-porosity material and a monoporous material and simulate the permittivity response based on the modeling approach described above for the dual-porosity configuration. The described model is compared to the *Topp et al.* [1980] empirical calibration for soils for a monoporous granular material:

$$\varepsilon_b = 3.03 + 9.30 \cdot \theta + 146 \cdot \theta^2 - 76.7 \cdot \theta^3. \quad (7)$$

In the case of the dual-porosity medium the SWA configuration dominates where the intra-aggregate pores are filling with water (stage 2), where the water content is between 0 and 0.4. The layered description dominates once all the intra-aggregate pores are water saturated (stage 4) and the interaggregate pores are filling, at water contents ranging from 0.4 to 0.8. Tangent lines are placed on the WRC for the dual-porosity medium indicating θ_{hc}, where the phase configuration changes from an SWA arrangement to a layered system.

[13] Note that the forgoing discussion applies to draining aggregated media. For the wetting case, the capillary fringe (dependent on aggregate size) and relatively tall sample will likely create a differently layered dielectric system than that depicted in Figure 1 (e.g., combination of 1, 4 and 5), likely leading to a different measurement outcome.

3. Materials and Methods

3.1. Aggregate Samples and Properties

[14] Four different aggregated porous media were considered in this study; zeoponic 0.25–1.0 mm (Rocky Mountain Zeolites LLC, Golden, Colorado), turface 2.0–5.0 mm (Aimcor, Deerfield, Illinois), profile 0.25–0.85 mm (Aimcor, Deerfield, Illinois), and pumice 3.2–9.5 mm (Charley's Greenhouse and Garden, Mount Vernon, Washington). Turface and profile are stabilized baked ceramic aggregates, with different aggregate sizes [*Steinberg et al.*, 2005]. The zeoponic is a mixture of zeolite (clinoptilolite) and rock phosphate (apatite) [*Steinberg et al.*, 2000]. The pumice is of volcanic origin from the Washington State area.

[15] The particle density of the solid fraction (ρ_s) comprising the aggregated media (Table 1) was determined via the pycnometer method using a volumetric flask [*Flint and Flint*, 2002]. The hygroscopic water content (θ_b) of each aggregated medium was determined by measuring the amount of water adsorbed at a relative humidity (p/p_0) of 0.19 by placing approximately 10 g of oven dry sample in a vacuum desiccation chamber over a saturated solution of calcium bromide ($CaBr_2$) at 20°C [*Quirk*, 1955; *Quirk and Murray*, 1999]. The amount of dry $CaBr_2$ required to produce a saturated solution was taken from *Weast* [1986]. After sample equilibration in the desiccation chamber, water content was determined via the thermogravimet-

Table 1. Measured Physical Properties and Chemical Compositions of the Four Aggregated Porous Media

Physical Property	Turface	Profile	Pumice	Zeoponic
Aggregate size range, mm	2.0–5.0	0.25–0.85	3.2–9.5	0.25–1.0
Particle density ρ_s, g cm^{-3}	2.5	2.5	2.1	2.5
Bulk density ρ_b, g cm^{-3}	0.62	0.65	0.36	0.97
Porosity ϕ	0.75	0.74	0.83	0.61
Saturated water content θ_s	0.75	0.75	0.82	0.58
Hydraulic critical water content θ_{hc}	0.34	0.32	0.47	0.21
Dielectric critical water content θ_{dc}	0.29	0.28	0.42	0.11
Connectivity ratio $(1 - \theta_{dc}/\theta_{hc})$	0.15	0.12	0.11	0.48
Hygroscopic water content, g_{water}/g_{soil}	0.018	0.019	0.0061	0.047
Hygroscopic water content θ_b	0.011	0.012	0.0022	0.045
Estimated surface area (SA), m^2 g^{-1}	55	56	18	140
Macropore fraction	0.56	0.57	0.43	0.64
Micropore fraction	0.44	0.43	0.57	0.36

Chemical Composition[a]	Turface	Pumice	Dark Zeoponic[b]	Light Zeoponic[b]
Si	38.55	37.06	36.91	6.16
O	34.46	15.44	45.11	34.64
Al	10.53	5.64	7.58	<2.00
Fe	2.18	32.04	<2.00	2.09
Mg	<2.00	7.23	<2.00	<2.00
K	11.60	2.59	6.15	<2.00
P	–	–	–	16.68
Ca	<2.00	–	<2.00	32.27

[a]All values are percentages. The detection limits of the EDS system were 2.00%.
[b]The dark and light zeoponic correspond to the two different shades of material observed in the scanning electron micrographs (Figure 8g). The dark and light materials comprise approximately 70 and 30% of the total, respectively.

ric method by drying the samples in an oven at 105°C for 24 hours [*Topp and Ferré*, 2002].

[16] Examination of the pore space in the aggregates was conducted using thin sections of the materials (Figure 2). The four aggregate materials were prepared by impregnation with epoxy, EPO-TEK 301 (Epoxy Technology Inc., Billerica, MA). After hardening, a 3.5×2.5 cm thin section was cut, mounted on a glass slide and polished. In the polishing process, a series of diamond polishers were used to avoid introduction of contaminants; no water was present.

[17] Thin sections were observed under a field emission scanning electron microscope (SEM) (Philips XL30 ESEM-FEG) using a backscatter electron detector. The intensity of the back-scattered electrons is a function of the atomic weight of the element, with heavier elements having higher back-scattering properties. Charging effects are counteracted by using low vacuum in the specimen chamber and by the introduction of water molecules to dissipate the charge accumulated on the surface of the sample; no coating was needed. Chemical analysis was conducted using the EDAX Phoenix (EDAX/TSL; Draper, UT) EDS system (Table 1).

3.2. Water Retention Characteristic Determination

[18] Water retention characteristic (WRC) determination was accomplished using a variety of methods corresponding to different matric potential ranges. The hanging water column method [*Dane and Hopmans*, 2002a] was used to measure the range between 0.0 and −0.3 m. The height of the samples in the suction apparatus [*Haines*, 1930] was small (≤2.0 cm), thus the variation in head from the top to the bottom of the sample was neglected. Water content of the samples was determined via monitoring the outflow volume with a burette.

[19] The pressure plate extractor method [*Dane and Hopmans*, 2002b] was used to measure the matric potential range between −1.0 and −100 m. Samples on the pressure plate were contained in 1.0 cm tall rings and the pressure was measured with a mercury manometer for measurements between −1.0 and −10 m and a pressure gauge for measurements <−10 m. After sample equilibration in the pressure chamber, water content was determined via the thermogravimetric method by drying the samples in an oven at 105°C for 24 hours [*Topp and Ferré*, 2002].

[20] A Dew Point Potentiometer (Decagon Devices, Inc., Pullman, WA) was used according to the method described by *Scanlon et al.* [2002] to measure the water potential values in the range of matric potential <−100 m. Pore water
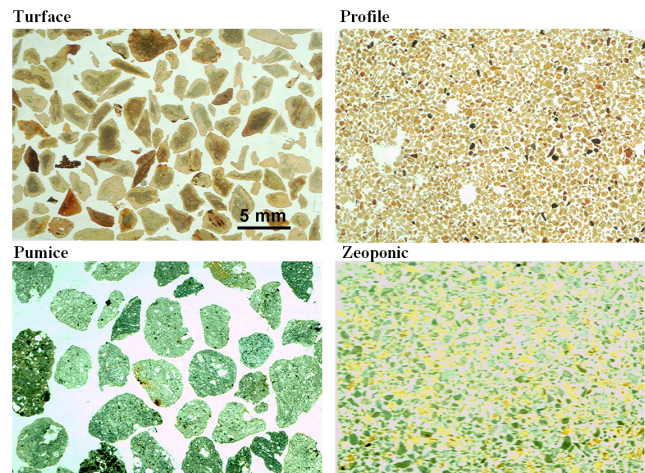

Figure 2. Thin-sectioned aggregates illustrating the size, distribution, and structure of the four aggregates considered.

Table 2. van Genuchten Parameters for the Four Aggregate Media Samples[a]

Parameter	Turface	Profile	Pumice	Zeoponic
Residual water content (θ_r)	0.00	0.00	0.005	0.027
Interaggregate pores				
α, cm^{-1}	27.0	6.56	377	8.14
n	2.78	7.01	2.41	6.92
Intra-aggregate pores				
α, cm^{-1}	0.00378	0.00518	0.584	0.00194
n	1.73	1.63	1.71	1.54

[a]Values for the saturated water content (θ_s) and hydraulic critical water content (θ_{hc}) are given in Table 1. The parameters α and n are curve fitting parameters relating to the matric head at air entry and pore size distribution, respectively.

electrical conductivities of each sample were <1.7 dS m^{-1}, thus solute effects were considered negligible compared to matric forces and the measured water potential was assumed to equal the matric potential. After potential measurement, water content was determined via the thermogravimetric method by drying the samples in an oven at 105°C for 24 hours [*Topp and Ferré*, 2002].

[21] The four aggregate samples considered were all characterized by a bimodal WRC owing to their dual-pore nature. The measured WRC data were modeled using a bimodal function consisting of superpositioned van Genuchten retention functions [*Durner*, 1994; *Kosugi et al.*, 2002] (equation (1)) (parameters are listed in Table 2). The cutoff point between interaggregate pores and intra-aggregate pores, θ_{hc}, was found to be $h = -10$ m for the turface, profile and zeoponic samples, and $h = -0.1$ m for the pumice sample.

3.3. Water Content–Permittivity Measurements

[22] Time domain reflectometry (TDR) measures the traveltime (t) of a broadband EM signal propagating along the probe embedded in the medium and relates t to apparent permittivity, which can then be related to θ. Calculation of TDR-estimated apparent permittivity (K_{TDR}) (= real permittivity (ε') in lossless media) from t [s] measurements is accomplished according to

$$K_{TDR} = \left(\frac{ct}{2L_e}\right)^2 \qquad (8)$$

where c is the speed of light in vacuum (3×10^8 m s^{-1}) and L_e is the apparent length of the probe [m]. The signal is reflected at the end of the probe and the return signal is sampled. The factor 2 in the denominator of equation (8) accounts for the two-way (down and back) traveltime of the signal.

[23] Permittivity measurements with TDR were made using custom designed measurement cells (Figure 3). The cell design is fundamental to the success of high-quality measurements. The sampling volume of a TDR probe is dependent on probe design [*Knight*, 1992]. Parallel plates were chosen to provide a uniform energy density between them, removing bias due to the sampling volume associated with the electrode design. *Robinson and Friedman* [2000] demonstrated that permittivity measurement using cylindrical rods can cause bias in the sampling volume due to the skin effect; this is substantially reduced using parallel plates, offering a more representative measurement.

[24] The TDR measurement cells consist of an 18.0 cm tall, 8.9 cm inner diameter plastic cylinder mounted on a 12.0×12.0 cm Plexiglas base, which serves as the medium containment chamber. The base has a 8.9 cm diameter cylindrical portion extending 2.0 cm above the 12.0×12.0 cm section and the plastic cylinder fits over the top of the cylindrical portion of the base, which uses an O-ring to prevent leakage. The containment chamber volume is approximately 950 cm^3. Two parallel, stainless steel plates were used as electrodes for the TDR probe and were mounted in the Plexiglas base with epoxy so as to extend into the medium containment chamber. Within the epoxy the plates were soldered to the end of a 0.5 m length of RG-58 coaxial cable. The plates are 15.3 cm in length, 2.5 cm in width and are spaced 2.0 cm apart. The parallel plate probe in each cell was calibrated according to the air and water method described by *Robinson et al.* [2003a]. The
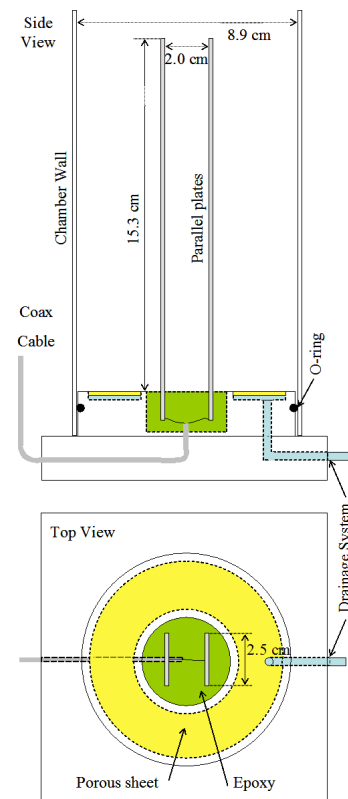

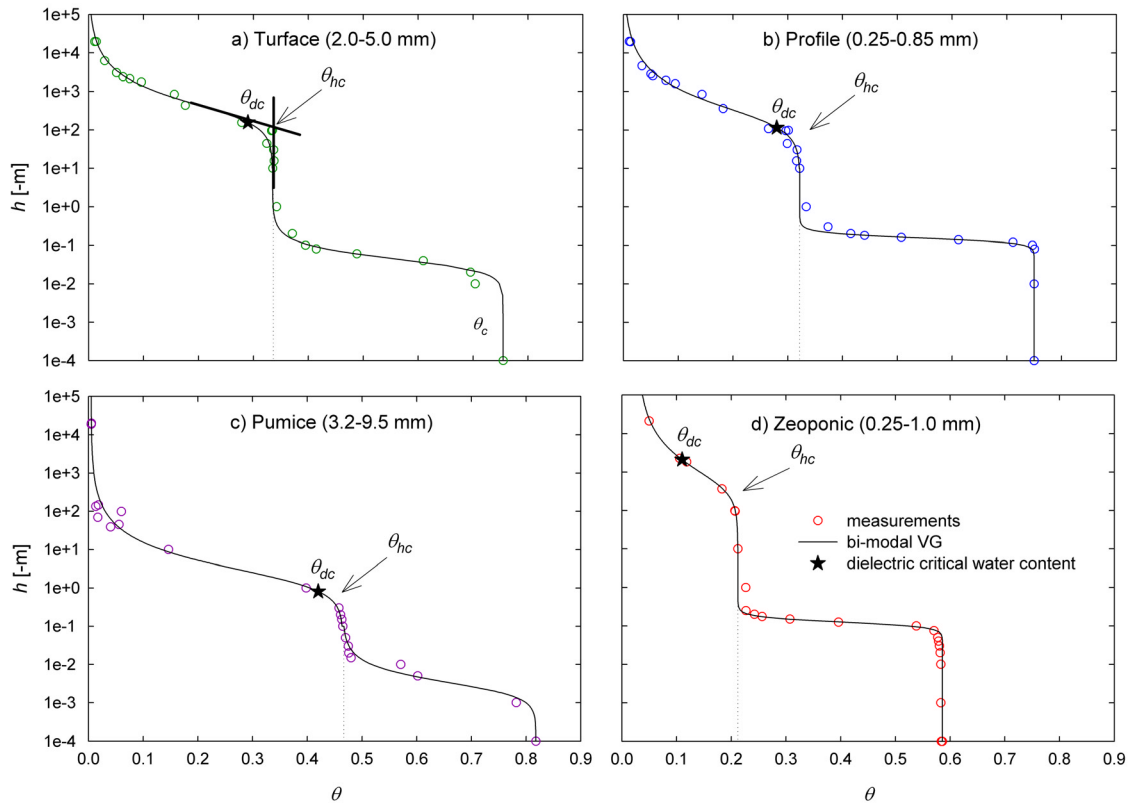**Figure 3.** Schematic drawing of the described custom measurement cell.

Figure 4. Water retention characteristics (WRCs) for (a) turface, (b) profile, (c) pumice, and (d) zeoponic. Bimodal van Genuchten model (equation (1)) is fit to the measured WRC data (parameters are listed in Table 2). The match point for the bimodal WRC model is matric head equal to -10 m for turface, profile, and zeoponic and -0.1 m for pumice. The dielectric critical water content value (θ_{dc}) corresponds to the change in slope of the $\theta - K_{TDR}$ relationships (Figure 6), and the hydraulic critical water content (θ_{hc}) corresponds to the stage where the interaggregate pores are dry and the intra-aggregate pores are saturated (Figure 1).

cylindrical portion of the base was recessed in a ring shape around the parallel plates and a piece of sintered plastic sheet with 7.0 μm pore size and 0.635 mm thickness (X-7744 T3 sheet, Porex Porous Products Group, Fairburn, GA) was glued into the recessed ring. A tube leading from under the porous sheet allowed the cell to be drained and wetted through the sheet. In order to make the sintered plastic sheet hydrophilic it was soaked with a surfactant consisting of 20 % Tween 20® (Sigma-Aldrich Co., St. Louis, MO) and 80 % isopropyl alcohol, then allowed to dry for approximately 30 minutes and rinsed with deionized water.

[25] Permittivity determinations (equation (8)) were carried out under temperature controlled conditions (24 ± 0.5°C) in the four aggregate media samples described above. Saturation of the samples was accomplished by mixing the media in a NaCl solution (electrical conductivity ≈0.5 dS m^{-1}) and placing the mixture under vacuum for approximately four hours. After each sample was saturated, the cell was packed with sample via tapping on a solid bench surface to achieve tight packing. Water content was monitored by measuring the loss in mass of the cell during drainage. The ϕ of each sample was independently verified using ρ_s and ρ_b measurements (Table 1) and found to correspond to the saturated water contents (θ_s) to better than 0.01 for turface, profile and pumice, and 0.03 for zeoponic (Table 1). Multiple measurements were taken as

water was removed from the samples via draining through the sintered plastic sheet and drying in an oven at 80°C to remove any remaining water (the plastic components of the cell are sensitive to 105°C temperatures). Measurements were made with a standard TDR cable tester (Tektronix Inc., Beaverton, OR; 1502B Metallic Cable Tester) and waveforms were captured with the use of WinTDR 6.0 waveform analysis software [Or et al., 2003].

4. Results and Discussion

4.1. Material Properties and Water Retention Characteristics

[26] The physical properties measured for each of the four aggregated media considered are presented in Table 1. The high porosity leads to exceptionally low bulk densities (<1 g cm^{-3}) Values such as this are often found in volcanic and tropical soils [Sanchez, 1976] and might be a good first indicator of dual-porosity systems. The hygroscopic water content (θ_b) in the materials was low, other than in the zeoponic, which had a value of 0.045. The measured and modeled WRCs are presented in Figures 4a–4d, with the value determined for θ_{hc} indicated by an arrow and vertical dotted line. Clearly, all materials exhibit a strong dual-porosity nature. The bimodal van Genuchten model (equation (1)) was found to describe the data well.
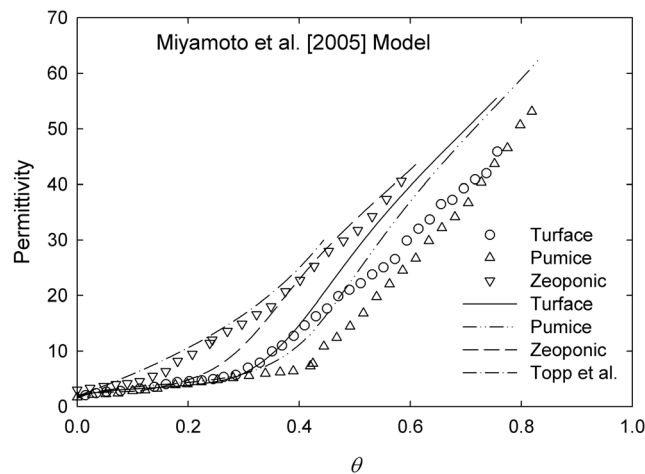
Figure 5. The *Miyamoto et al.* [2005, equations (4)–(9) and (11)–(13)] model fit to the measured $\theta - K_{TDR}$ data for turface (RMSE = 5.91), pumice (RMSE = 7.06), and zeoponic (RMSE = 3.02). The model is shown not to fit the data very well, likely owing to the weighting functions used by *Miyamoto et al.* [2005] for Andisols. The *Topp et al.* [1980] (equation (7)) empirical calibration for mineral soils is shown for reference.

4.2. Water Content–Permittivity Modeling

[27] As a first step we compared the measured $\theta - K_{TDR}$ results with model predictions based on the extended dual-composite sphere model (DCSM) presented by *Miyamoto et al.* [2005, equations (4)–(9) and (11)–(13)] for Andisols (Figure 5). We used a value of 5 for the solid permittivity based on the mineralogy being dominated by alumino-silicate material (Table 1) and the permittivity values determined for such materials by *Robinson* [2004]. Values for the surface area were not available, but were estimated based on the bound water fraction on a mass basis (i.e., $g_{water}\, g_{soil}^{-1}$). This resulted in surface areas ranging from 18 m^2 g^{-1} for pumice to 140 m^2 g^{-1} for zeoponic (Table 1). This assumes monolayer coverage of water and an area of 9 square angstroms per water molecule. Water is not an ideal probe molecule because of its considerable polarity [*Quirk and Murray*, 1999]; however, the Miyamoto et al. DCSM model is not particularly sensitive to the quantity of bound water so broad latitude can be given to these values without it impacting the result very much. The model does a poor job of predicting the behavior of these aggregated materials other than at low water contents (Figure 5). The DCSM model was developed to describe Andisols that have a mineralogy dominated by Allophane. Allophane is characterized in its composition by hollow spheres that together form aggregates [*Wada*, 1989]. The Miyamoto et al. DCSM four-phase concentric sphere description of this material is a reasonable approximation of the material; however, they had to fit empirical weighting functions to the model in order to describe the behavior of the Andisols they measured. The poor fit with our measurements indicates the poor general applicability of these weighting functions for the aggregated materials treated herein.

[28] In Figures 6a–6d we present the measured $\theta - K_{TDR}$ drainage curve data for all four aggregated materials. For the convenience of comparison we present the empirical calibration presented by *Topp et al.* [1980] for soils (equation (7)). Figure 6 also contains the predictions of the modeling approach outlined in the theory section; where model 1 uses equation (6) to calculate the permittivity from the dry end to the hydraulic critical water content (θ_{hc}) and then uses the layer model (equation (5)) to calculate the permittivity from θ_{hc} to saturation. The saturation permittivity (ε_{sat}) is determined from the double mixing using the Maxwell-Garnett formula (equation (4)). Model 2 uses this same approach but the position of the point where the slope in the $\theta - K_{TDR}$ relationship changes in the model is adjusted from the hydraulic critical water content (θ_{hc}) to the dielectric critical water content (θ_{dc}), which is determined from the point at which the measured $\theta - K_{TDR}$ data changes slope. The θ_{hc} and θ_{dc} values differ, the implications of which we consider later. The ε_s value (equations (4) and (6)) in the two models is assumed to be 5 for all media.

[29] The assumptions made in the modeling mean that the fit between the model and the data could be improved; however, the use of two descriptions of the drainage process clearly captures the two step trend in the data (Figure 6). In densely packed materials the model does not account for depolarization arising from field interactions between particles [*Sihvola and Kong*, 1988; *Robinson and Friedman*, 2005], nor does the model used account for particle shape [*Jones and Friedman*, 2000]. A methodology has been presented by *Friedman and Robinson* [2002] to account for these factors for granular materials; however, the complex geometry of the aggregates used in this study does not lend itself to this approach. As it stands the modeling behaves as we would expect based on the assumptions in the model of noninteracting particles, at saturation an upper bound is observed, and when dry a lower bound is observed. An upper bound is expected for a dielectric contrast $\varepsilon_i/\varepsilon_e < 1$ and a lower bound is expected when $\varepsilon_i/\varepsilon_e > 1$, where ε_i is inclusion permittivity and ε_e is environment permittivity [*Robinson and Friedman*, 2005]. The approach presented is therefore a first approximation designed to capture the general physics of the permittivity change as a function of drainage, and explain this behavior as a consequence of the change in the phase configuration.
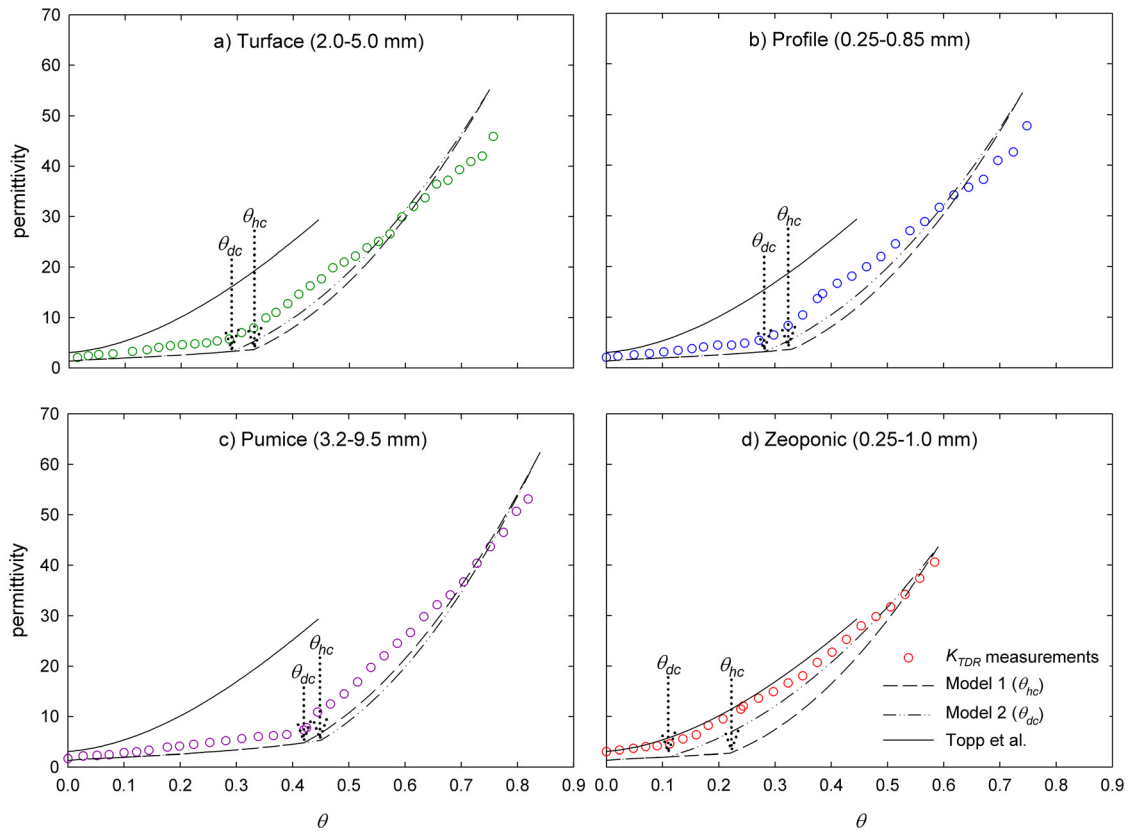
Figure 6. Model proposed in this work (equations (4)–(6)) fit to the measured $\theta - K_{TDR}$ data for each of the four aggregate samples. Model 1 is calculated with the hydraulic critical water content (θ_{hc}), and model 2 is calculated with the dielectric critical water content (θ_{dc}). The *Topp et al.* [1980] empirical calibration for mineral soils (equations (7)) is shown for reference.

[30] The critical point at which the change in the measured $\theta - K_{TDR}$ relationship occurs, θ_{dc}, is of some interest. The first approximation used in the model was θ_{hc}, occurring after the interaggregate pores had drained; however, by using equations (2) and (3), we can determine the effective pore size distribution as a function of effective pore radius (r) (Figure 7). In Figures 7a and 7b the dielectric critical points (θ_{dc}) are plotted based on the matric potential (h) at which they were observed and are related to pore size distribution as a function of r. Initial expectation was that θ_{dc} would fall to the right of the intra-aggregate pore curve, indicating that θ_{dc} occurred after the interaggregate pores had drained but before the intra-aggregate pores emptied. However, the data indicate that this is not the whole story. The θ_{dc} value for the pumice occurs after about 11% of the intra-aggregate pores have drained. In the case of the turface and profile the values are 15% and 12%, respectively. The θ_{dc} for zeoponic does not occur until approximately half the intra-aggregate pore space, 48%, has been emptied of water. This perhaps indicates that the internal structural arrangement differs greatly between the different materials.

[31] Electron micrographs of the pumice, turface and zeoponic (turface and profile are of the same parent material) are presented (Figure 8). The magnification increases from left to right. The pumice (Figures 8a–8c) is full of vesicles not accessible to water (likely contributes to ρ_s being much lower than the other media (Table 1)), which from Figure 8b are dominated by vesicles of a few μm and

extending to about 50 μm. These estimates approximate the pore size distribution determined from the WRC (Figure 7b). The wall material that has been broken and fractured during the grinding process is visible in Figure 8c. Both the turface and the zeoponic have structural arrangement that is on a much smaller scale. Both materials are composed of platy structures up to a few microns in length, creating pores that appear to be submicron (Figures 8f–8i), again in agreement with Figure 7b. However, closer inspection of the turface platy particles showed them to be discrete, whereas the zeoponic had a fine platy structure at the nanometer scale (Figure 9). The zeoponic material has a very fine internal platy structure that appeared to be highly interconnected (Figure 9). Our belief is that this structure is responsible for maintaining hydraulic, and therefore electrical, continuity within the intra-aggregate pore network even when much of the pore volume has been drained. The ratio between the dielectric critical water content and the hydraulic critical water content (θ_{dc}/θ_{hc}) is therefore an indicator of the intra-aggregate pore continuity and interconnectedness, we term $1-(\theta_{dc}/\theta_{hc})$ the connectivity ratio. This gives values ranging from 0.11 for the pumice to 0.48 for the zeoponic (Table 1), the closer the value to 0, the less connectivity of the intra-aggregate pore space. This ratio may be important in characterizing aggregated materials for understanding flow and transport at low levels of saturation where the aggregates are of similar size. A broader particle size distribution will alter this relationship.
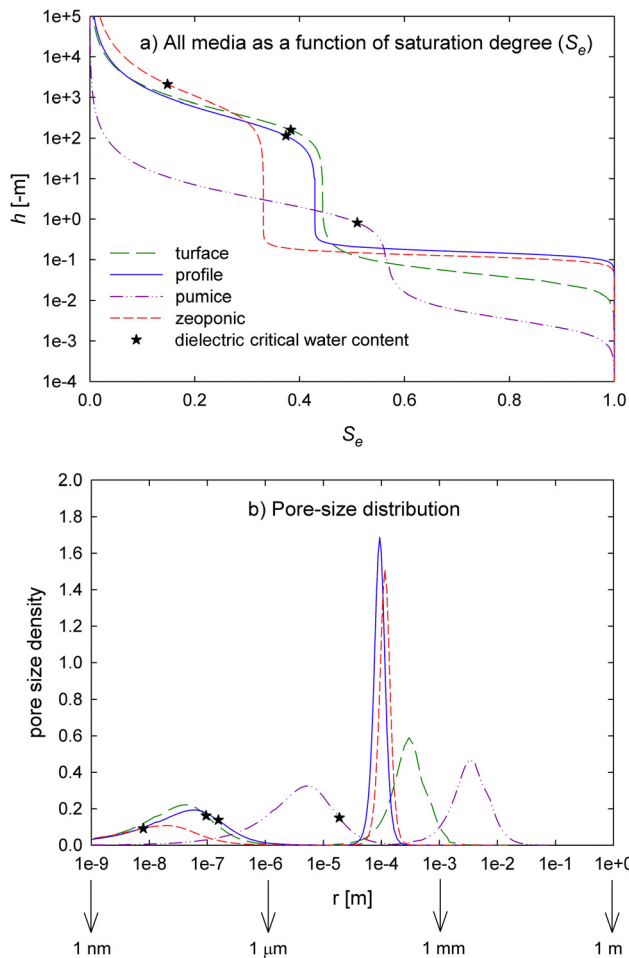
Figure 8. Scanning electron micrographs (SEMs) of the (a−c) pumice, (d−f) turface, and (g−i) zeoponic samples. The aggregates are depicted in Figures 8a, 8d, and 8g and are cross-sectional images. Zoomed-in views of the aggregate cross sections are shown in Figures 8b, 8e, and 8h and depict interaggregate surface morphological features. The internal aggregate structure is displayed in Figures 8c, 8f, and 8i and show intra-aggregate surface morphological features. The color contrast is due to density and chemical composition differences; the lighter colors are denser materials and vice versa (Table 1).

Figure 7. (a) Water retention characteristics (WRCs) for all four aggregated media as a function of saturation degree (S_e) and (b) pore size distributions for all four media. Bimodal van Genuchten model (equation (1)) is fit to the measured WRC data, and equations (2) and (3) determine the pore size distributions. The match point for the bimodal WRC model is matric head equal to -10 m for turface, profile, and zeoponic and -0.1 m for pumice. The dielectric critical water content (θ_{dc}) corresponds to the change in slope of the measured $\theta - K_{TDR}$ relationships (Figure 6).

[32] Regarding measurement scale, we note that results presented here are dependent on a vertically oriented TDR probe in a porous aggregated system whose water level in the interaggregate pores is changing perpendicular to the probe, according to the layered system described by *Robinson et al.* [2005]. For a horizontally oriented probe in highly aggregated media, the $\theta - K_{TDR}$ relationship may be modified due to the different signal averaging where signal propagation is parallel to the layering (e.g., water content variation with depth). *Jones and Friedman* [2000] compared vertical and horizontal probe orientations and noted only slight differences in the $\theta - K_{TDR}$ relationship for spherical grain packs, while in layered platy particle packs a doubling in K_{TDR} for a vertically oriented probe was observed compared to the horizontal orientation. Measured $\theta - K_{TDR}$ relationships for individual aggregates should appear like the monosized pore system shown in Figure 1,
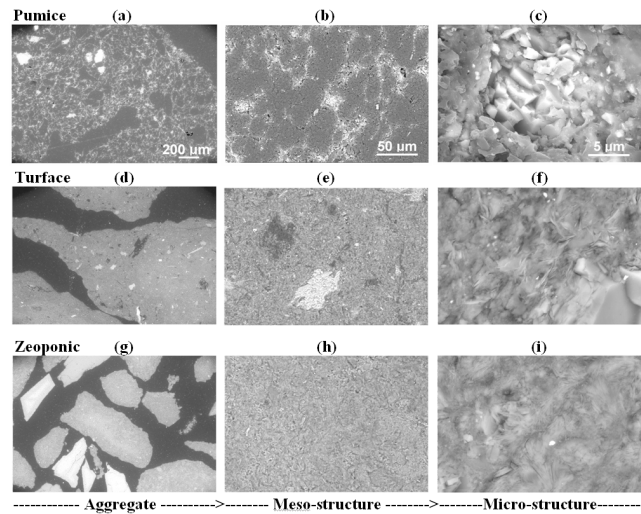
but with potentially reduced K_{TDR} values relative to the *Topp et al.* [1980] equation (equation (7)), owing to the combined phase configuration and water-binding effects.

4.3. Bound Water Versus Phase Configuration

[33] Many empirical and semiphysical dielectric mixing models have emphasized the role of bound water in creating deviations from the Topp et al. calibration equation. However, the original data from Topp et al. indicated the
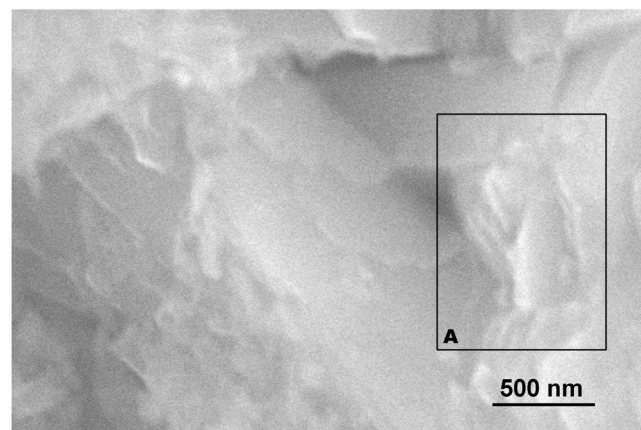

Figure 9. Nanometer-scale scanning electron micrograph (SEM) showing the internal aggregate structure of the zeoponic. The edge of the platy nanometer-scale structure is shown (A).

important role of structure as their empirical calibration for vermiculite fell well below that of the mineral soils [*Topp et al.*, 1980]. More recent work has also indicated the important role of structure on the dielectric – water content relationship [*Friedman*, 1998; *Jones and Or*, 2002]. An important problem that has yet to be solved is quantifying the relative contributions of bound water and structure to the $\theta - \varepsilon_b$ relationship. The existence of bound water is not in doubt, and there is much evidence from temperature and frequency effects in porous media that indicate bound water is a contributing factor to permittivity reductions in the $\theta - \varepsilon_b$ relationship [*Wraith and Or*, 1999; *Or and Wraith*, 1999]. In Debye's Nobel prize publication [*Debye*, 1929] he calculated the expected dielectric saturation of a water molecule in the presence of a cation. More recently, *Hasted et al.* [1948] characterized the dielectric decrement for a range of aqueous electrolytes. In the last twenty years bound water has become a convenient fitting parameter in many dielectric models of soils [*Dobson et al.*, 1985; *Dirksen and Dasberg*, 1993; *Robinson et al.*, 2001], but there has been little direct evidence of the amount by which the permittivity of water at surfaces might be reduced compared to free water. Literature estimates for values determined indirectly range between 3.2 [*Dirksen and Dasberg*, 1993] and 41 [*Thorp*, 1959]; 4.3 is probably a more physically realistic lower bound corresponding to the high-frequency permittivity (ε_∞) of water [*Hasted*, 1973].

[34] As an alternative hypothesis, we propose that the reductions in observed permittivity for the described aggregates are caused by pore connectivity. We base this hypothesis on the data obtained from the zeoponic and pumice. *Quirk* [1955] found that monolayer coverage of the solid phase by one layer of water molecules, occurs at a relative humidity (p/p_0) = 0.19, and has suggested that measurements made at this partial pressure are a good indication of the quantity of hygroscopic water in a material [*Quirk and Murray*, 1999]. Thus our reported θ_b measurements (Table 1) should be indicative of the quantity of water that might be considered to be bound in the dielectric sense. Comparing the $\theta - K_{TDR}$ data for the zeoponic and pumice (Figures 5 and 6), we see the reverse of what we would expect if bound water accounted for a reduction in ε_b. The zeoponic with $\theta_b \approx 0.05$ compares closely to the Topp et al. calibration, whereas the pumice, with $\theta_b < 0.01$, deviates the most from the Topp et al. calibration. We have presented an argument based on the structural water configuration to account for this. Therefore we speculate that in many cases the reduction in permittivity observed in materials such as clays, which are composed of platy grains, could be accounted for in part by structural arrangement at the microscale. The nonrigid structure of many clay minerals, and their ability to shrink and swell, might maintain connectivity between interaggregate pores to low water contents. This may have important implications for the interpretation of $\theta - \varepsilon_b$ data. Where as the reduction has previously been assumed to indicate water bound in the dielectric sense in the radio and microwave frequency ranges, which is not immensely useful; it may alternatively indicate microgeometrical particle arrangement and its level of connectivity. This information could be of much greater utility in characterizing the flow and transport behavior of porous media. An important research goal must be to discriminate between the contributions of the microstructure and rotationally hindered water to ε_b.

5. Conclusions

[35] Many of the natural porous media in which we wish to determine water content; soils, sediments and rocks; are aggregated and characterized by dual-porosity pore networks, consisting of both interaggregate pores and intra-aggregate pores. We present measurements of permittivity as a function of water content for four aggregated materials. A two component model is used to describe the data based on the configuration of the water and air phases. The model links the dielectric response to the water retention characteristic of the media. The hydraulic critical water content (θ_{hc}) is defined as the point at which all the interaggregate pores are air filled and all the intra-aggregate pores are water saturated. Comparison between measurements shows that θ_{hc} and the dielectric critical water content (θ_{dc}) differ, the difference being considered to be a function of the connectivity of the intra-aggregate pore network. A connectivity ratio is defined as $1-(\theta_{dc}/\theta_{hc})$, where values close to 0 indicate low connectivity between the intra-aggregate pores and values tending to 1 indicate a high level of pore connectivity. Data for two of the materials, zeoponic and pumice, suggests that bound water is not responsible for deviation from the Topp et al. calibration for soils in the case of these samples. While we do not doubt the presence of dielectrically bound water under some circumstances, our measured data suggest that phase configuration plays an important role in determining the dielectric response of the sample. Further work must aim toward quantifying and defining the relative contributions of both bound water and confined water due to microstructure to the bulk dielectric response.

References

Alumbaugh, D., P. Y. Chang, L. Paprocki, J. R. Brainard, R. J. Glass, and C. A. Rautman (2002), Estimation of moisture contents in the vadose zone using cross-borehole ground penetrating radar: A study of accuracy and repeatability, *Water Resour. Res.*, *38*(12), 1309, doi:10.1029/2001WR000754.

Binley, A., P. Winship, R. Middleton, M. Pokar, and J. West (2001), High-resolution characterization of vadose zone dynamics using cross-borehole radar, *Water Resour. Res.*, *37*, 2639–2652.

Blonquist, J. M., Jr., S. B. Jones, and D. A. Robinson (2005), A time domain transmission sensor with TDR performance characteristics, *J. Hydrol.*, *314*, 235–245.

Blumberg, D. G., V. Freilikher, I. V. Lyalko, L. D. Vulfson, A. L. Kotlyar, V. N. Shevchenko, and A. D. Ryabokoneko (2000), Soil moisture (water-content) assessment by an airborne scatterometer: The Chernobyl disaster area and the Negev Desert, *Remote Sens. Environ.*, *71*, 309–319.

Bridge, B. J., J. Sabburg, K. O. Habash, J. A. R. Ball, and N. H. Hanock (1996), The dielectric behaviour of clay soils and its application to time domain reflectometry, *Aust. J. Soil Resour.*, *34*, 825–835.

Chanzy, A., A. Tarussov, A. Judge, and F. Bonn (1996), Soil water content determination using a digital ground-penetrating radar, *Soil Sci. Soc. Am. J.*, *60*, 1318–1326.

Cosenza, P., and A. Tabbagh (2004), Electromagnetic determination of clay water content: Role of the microporosity, *Appl. Clay Sci.*, 26(1–4), 21–36.

Cosenza, P., C. Camerlynck, and A. Tabbagh (2003), Differential effective medium schemes for investigating the relationship between high-frequency relative dielectric permittivity and water content of soils, *Water Resour. Res.*, 39(9), 1230, doi:10.1029/2002WR001774.

Dane, J. H., and J. W. Hopmans (2002a), Hanging water column, in *Methods of Soil Analysis*, part 4, *Physical Methods*, edited by J. H. Dane and G. C. Topp, pp. 680–684, Soil Sci. Soc. of Am., Madison, Wis.

Dane, J. H., and J. W. Hopmans (2002b), Pressure plate extractor, in *Methods of Soil Analysis*, part 4, *Physical Methods*, edited by J. H. Dane and G. C. Topp, pp. 688–690, Soil Sci. Soc. of Am., Madison, Wis.

Dean, T. J., J. P. Bell, and A. J. B. Baty (1987), Soil moisture measurement by an improved capacitance technique, part I. Sensor design and performance, *J. Hydrol.*, 93, 67–78.

Debye, P. (1929), *Polar Molecules*, Chem. Cat. Co., New York.

Dirksen, C., and S. Dasberg (1993), Improved calibration of time domain reflectometry soil water content measurements, *Soil Sci. Soc. Am. J.*, 57, 660–667.

Dobson, M. C., F. T. Ulaby, M. T. Hallikainen, and M. A. El-Rayes (1985), Microwave dielectric behavior of wet soil: Part II. Dielectric mixing models, *IEEE Trans. Geosci. Remote Sens.*, 23, 35–46.

Du, Y., F. T. Ulaby, and M. C. Dobson (2000), Sensitivity to soil moisture by active and passive microwave sensors, *IEEE Trans. Geosci. Remote Sens.*, 38, 105–114.

Dubois, P. C., J. van Zyl, and T. Engman (1995), Measuring soil moisture with imaging radars, *IEEE Trans. Geosci. Remote Sens.*, 33, 915–926.

Durner, W. (1994), Hydraulic conductivity estimation for soils with heterogeneous pore structure, *Water Resour. Res.*, 30, 211–223.

Flint, A. L., and L. E. Flint (2002), Particle density, in *Methods of Soil Analysis*, part 4, *Physical Methods*, edited by J. H. Dane and G. C. Topp, pp. 229–240, Soil Sci. Soc. of Am., Madison, Wis.

Friedman, S. P. (1998), A saturation degree-dependent composite spheres model for describing the effective dielectric constant of unsaturated porous media, *Water Resour. Res.*, 34, 2949–2961.

Friedman, S. P., and S. B. Jones (2001), Measurement and approximate critical path analysis of the pore-scale-induced anisotropy factor of an unsaturated porous medium, *Water Resour. Res.*, 37, 2929–2942.

Friedman, S. P., and D. A. Robinson (2002), Particle shape characterization using angle of repose measurements for predicting the effective permittivity and electrical conductivity of saturated granular media, *Water Resour. Res.*, 38(11), 1236, doi:10.1029/2001WR000746.

Gaskin, G. J., and J. D. Miller (1996), Measurement of soil water content using a simplified impedance measuring technique, *J. Agric. Eng. Res.*, 63, 153–159.

Haines, W. B. (1930), The hysteresis effect in capillary properties and the modes of moisture distribution associated therewith, *J. Agric. Sci.*, 20, 96–105.

Hasted, J. B. (1973), *Aqueous Dielectrics*, CRC Press, Boca Raton, Fla.

Hasted, J. B., D. M. Ritson, and C. H. Collie (1948), Dielectric properties of aqueous solutions. Part I, *J. Chem. Phys.*, 16, 1–11.

Hilhorst, M. A., J. Balendonck, and F. H. W. Kampers (1993), A broadbandwidth mixed analog/digital integrated circuit for the measurement of complex impedances, *IEEE J. Solid State Circuits*, 28, 764–769.

Hoekstra, P., and A. Delaney (1974), Dielectric properties of soils at UHF and microwave frequencies, *J. Geophys. Res.*, 79, 1699–1708.

Huisman, J. A., C. Sperl, W. Bouten, and J. M. Verstraten (2001), Soil water content measurements at different scales: Accuracy of time domain reflectometry and ground-penetration radar, *J. Hydrol.*, 245, 48–58.

Ishida, T., and T. Makino (1999), Effects of pH on dielectric relaxation of montmorillonite, allophone, and imogolite suspensions, *J. Colloid Interface Sci.*, 212, 152–161.

Jacobsen, O. H., and P. Schjønning (1993), A laboratory calibration of time domain reflectometry for soil water measurement including effects of bulk density and texture, *J. Hydrol.*, 151, 147–158.

Jones, S. B., and S. P. Friedman (2000), Particle shape effects on the effective permittivity of anisotropic or isotropic media consisting of aligned or randomly oriented ellipsoidal particles, *Water Resour. Res.*, 36, 2821–2833.

Jones, S. B., and D. Or (2002), Surface area, geometrical and configurational effects on permittivity of porous media, *J. Non Crystalline Solids*, 305, 247–254.

Jones, S. B., J. M. Wraith, and D. Or (2002), Time domain reflectometry measurement principles and applications, *Hydrol. Processes*, 16, 141–153.

Kelleners, T. J., R. O. W. Soppe, D. A. Robinson, M. G. Schaap, J. E. Ayers, and T. H. Skaggs (2004), Calibration of capacitance probe sensors using electric circuit theory, *Soil Sci. Soc. Am. J.*, 68, 430–439.

Knight, J. H. (1992), Sensitivity of time domain reflectometry measurements to lateral variations in soil water content, *Water Resour. Res.*, 28, 2345–2352.

Kosugi, K., J. W. Hopmans, and J. H. Dane (2002), Parametric models, in *Methods of Soil Analysis*, part 4, *Physical Methods*, edited by J. H. Dane and G. C. Topp, pp. 739–755, Soil Sci. Soc. of Am., Madison, Wis.

Lesch, S. M., D. L. Corwin, and D. A. Robinson (2005), Apparent soil electrical conductivity mapping as an agricultural management tool in arid zone soils, *Comput. Electron. Agric.*, 46, 351–378.

Logsdon, S. D. (2005), Soil dielectric spectra from vector network analyzer data, *Soil Sci. Soc. Am J.*, 69, 983–989.

Malicki, M. A., R. Plagge, and C. H. Roth (1996), Improving the calibration of dielectric TDR soil moisture determination taking into account the solid soil, *Eur. J. Soil Sci.*, 47, 357–366.

Maxwell-Garnett, J. C. (1904), Colours in metal glasses and in metallic films, *Philos. Trans. R. Soc. London, Ser. A*, 203, 385–420.

Miyamoto, T., A. Takeyuki, and J. Chikushi (2003), Soil aggregate structure effects on dielectric permittivity of an Andisol measured by time domain reflectometry, *Vadose Zone J.*, 2, 90–97.

Miyamoto, T., A. Takeyuki, and J. Chikushi (2005), Extended dual composite sphere model for determining dielectric permittivity of Andisols, *Soil Sci. Soc. Am. J.*, 69, 23–29.

Noborio, K. (2001), Measurement of soil water content and electrical conductivity by time domain reflectometry: A review, *Comput. Electron. Agric.*, 31, 213–237.

Or, D., and J. M. Wraith (1999), Temperature effects on soil bulk dielectric permittivity measured by time domain reflectometry: A physical model, *Water Resour. Res.*, 35, 371–383.

Or, D., S. B. Jones, J. R. VanShaar, and J. M. Wraith (2003), WinTDR 6.0 users guide (Windows-based TDR program for soil water content and electrical conductivity measurement), report, Utah Agric. Exp. Stn. Res., Logan. (Available at http://soilphysics.usu.edu/wintdr/documentation.htm)

Palmer, L. S. (1952), On the dielectric constant of water in wet clay, *Proc. Phys. Soc. London, Sect. B*, 65(9), 674–678.

Paltineanu, I. C., and J. L. Starr (1997), Real-time soil water dynamics using multisensor capacitance probes: Laboratory calibration, *Soil Sci. Soc. Am. J.*, 61, 1576–1585.

Quirk, J. P. (1955), Significance of surface areas calculated from water vapor sorption isotherms by use of the B.E.T. equation, *Soil Sci.*, 80, 423–430.

Quirk, J. P., and R. S. Murray (1999), Appraisal of ethylene glycol monoethyl ether method for measuring hydratable surface area of clays and soils, *Soil Sci. Soc. Am. J.*, 63, 839–849.

Robinson, D. A. (2004), Measurement of the solid dielectric permittivity of clay minerals and granular samples using a time domain reflectometry immersion method, *Vadose Zone J.*, 3, 705–713.

Robinson, D. A., and S. P. Friedman (2000), Parallel plates compared with conventional rods as TDR waveguides for sensing soil moisture, *Subsurface Sens. Technol. Appl.*, 1, 497–511.

Robinson, D. A., and S. P. Friedman (2001), Effect of particle size distribution on the effective dielectric permittivity of saturated granular media, *Water Resour. Res.*, 37, 33–40.

Robinson, D. A., and S. P. Friedman (2005), Electrical conductivity and dielectric permittivity of sphere packings: Measurements and modeling of cubic lattices, randomly packed monosize spheres and multi-size mixtures, *Physica A*, 358, 447–465.

Robinson, D. A., J. D. Cooper, and C. M. K. Gardner (2001), Modelling the relative permittivity of soils using soil hygroscopic water content, *J. Hydrol.*, 255, 39–49.

Robinson, D. A., M. Schaap, S. B. Jones, S. P. Friedman, and C. M. K. Gardner (2003a), Considerations for improving the accuracy of permittivity measurement using time domain reflectometry: Air-water calibration, effects of cable length, *Soil Sci. Soc. Am. J.*, 67, 62–70.

Robinson, D. A., S. B. Jones, J. M. Wraith, D. Or, and S. P. Friedman (2003b), A review of advances in dielectric and electrical conductivity measurement in soils using time domain reflectometry, *Vadose Zone J.*, 2, 444–475.

Robinson, D. A., S. B. Jones, J. M. Blonquist, Jr., and S. P. Friedman (2005), A physically based water content/permittivity calibration model for coarse-textured, layered soils, *Soil Sci. Soc. Am. J.*, 69, 1372–1378.

Roth, C. H., M. A. Malicki, and R. Plagge (1992), Empirical evaluation of the relationship between soil dielectric constant and volumetric water

content and the basis for calibrating soil moisture measurements by TDR, *J. Soil Sci.*, *43*, 1–13.

Sanchez, P. A. (1976), *Properties and Management of Soils in the Tropics*, John Wiley, Hoboken, N. J.

Scanlon, B. R., B. J. Andraski, and J. Bilskie (2002), Miscellaneous methods for measuring matric or water potential, in *Methods of Soil Analysis*, part 4, *Physical Methods*, edited by J. H. Dane and G. C. Topp, pp. 643–669, Soil Sci. Soc. of Am., Madison, Wis.

Seyfried, M. S., and M. D. Murdock (2004), Measurement of soil water content with a 50-MHz soil dielectric sensor, *Soil Sci. Soc. Am. J.*, *68*, 394–403.

Sihvola, A. H. (1999), *Electromagnetic Mixing Formulas and Applications*, Inst. of Electr. Eng., London.

Sihvola, A. H., and J. A. Kong (1988), Effective permittivity of dielectric mixtures, *IEEE Trans. Geosci. Remote Sens.*, *26*, 420–429.

Steinberg, S. L., D. W. Ming, K. E. Henderson, C. Carrier, J. E. Gruener, D. J. Barta, and D. L. Henninger (2000), Wheat response to differences in water and nutritional status between zeoponic and hydroponic growth systems, *Agron. J.*, *92*, 353–360.

Steinberg, S. L., G. Kluitenberg, S. B. Jones, N. Diadzic, L. Reddi, M. Xiao, M. Tuller, R. Newman, D. Or, and J. I. D. Alexander (2005), Physical and hydraulic properties of baked ceramic aggregates used for plant growth medium, *J. Am. Soc. Hortic. Sci.*, *130*(5), 767–774.

Stuchly, S. S. (1970), Dielectric properties of some granular solids containing water, *Microwave Power, J.*, *5*, 62–68.

Thorp, J. M. (1959), The dielectric behaviour of vapours adsorbed on porous solids, *Trans. Faraday Soc.*, *55*, 442–454.

Topp, G. C., and P. A. Ferré (2002), Thermogravimetric method using convective oven-drying, in *Methods of Soil Analysis*, part 4, *Physical Methods*, edited by J. H. Dane and G. C. Topp, p. 419, Soil Sci. Soc. of Am., Madison, Wis.

Topp, G. C., J. L. Davis, and A. P. Annan (1980), Electromagnetic determination of soil water content: Measurements in coaxial transmission lines, *Water Resour. Res.*, *16*, 574–582.

van Overmeeren, R. A., S. V. Sariowan, and J. C. Gehrels (1997), Ground penetrating radar for determining volumetric soil water content: Results of comparative measurements at two test sites, *J. Hydrol.*, *197*, 316–338.

Ulaby, F. T., C. D. Pascale, and J. van Zyl (1996), Radar mapping of surface soil moisture, *J. Hydrol.*, *184*, 57–84.

van Genuchten, M. T. (1980), A closed-form equation for predicting the hydraulic conductivity of unsaturated soils, *Soil Sci. Soc. Am. J.*, *44*, 892–898.

Wada, K. (1989), Allophane and Imogolite, in *Minerals in Soil Environments*, edited by J. B. Dixon and S. B. Weed, pp. 1051–1087, Soil Sci. Soc. of Am., Madison, Wis.

Weast, R. C. (Ed.) (1986), *CRC Handbook of Chemistry and Physics*, 67th ed., CRC Press, Boca Raton, Fla.

Wraith, J. M., and D. Or (1999), Temperature effects on soil bulk dielectric permittivity measured by time domain reflectometry: Experimental evidence and hypothesis development, *Water Resour. Res.*, *35*, 361–369.

Yu, C. W., A. W. Warrick, M. H. Conklin, M. H. Young, and M. Zreda (1997), Two- and three- parameter calibrations of time domain reflectometry for soil moisture measurement, *Water Resour. Res.*, *33*, 2417–2421.

————————————

J. M. Blonquist Jr. and S. B. Jones, Department of Plants, Soils and Biometeorology, Utah State University, 4820 Old Main Hill, Logan, UT 84322-4820, USA.

I. Lebron and D. A. Robinson, Department of Geophysics, Stanford University, 397 Panama Mall, Stanford, CA 94305-2215, USA. (darob@stanford.edu)